PCCP

Molecular Dynamics Evidence for Nonthermal Effects of Electric Fields on Pectin Methylesterase Activity

Journal:	*Physical Chemistry Chemical Physics*
Manuscript ID	CP-ART-11-2020-005950.R2
Article Type:	Paper
Date Submitted by the Author:	17-Jun-2021
Complete List of Authors:	Samaranayake, Chaminda; The Ohio State University Sastry, S.; Ohio State University,

Molecular Dynamics Evidence for Nonthermal Effects of Electric Fields on Pectin Methylesterase Activity

Chaminda P. Samaranayake[1], Sudhir K. Sastry[1,a]

[1] *Department of Food, Agricultural and Biological Engineering, The Ohio State University, 590 Woody Hayes Drive, Columbus, Ohio, 43210, United States*

[a] *Corresponding author*

Phone: 1 (614) 292-3508

Fax: 1 (614) 292-9448

E-mail: sastry.2@osu.edu

ABSTRACT

Experimental studies relevant to the nonthermal effects of electric fields on biological systems are emerging. However, these effects are poorly understood at the molecular level. The present study investigates pectin methylesterase, a cell wall modifying enzyme in plants, exposed to various electric field strengths. Molecular dynamics (MD) of the enzyme were studied with and without (thermal-only) electric field applications. The measurements were interpreted on the basis of equivalent energy input to gain insights into the effect of electric field treatment time at a constant temperature (50 °C). Results reveal that electric fields exert nonthermal effects on both local and global protein structure. In 1 μs simulations, the results show significant ($P \leq 0.05$) shrinkage of the catalytic domain and shortening of enzyme-water hydrogen bond lifetime by a 50 V/cm electric field. Unwinding of the helical segments, altered intra- and intermolecular hydrogen bond patterns, and increased hydration are also caused by the 50 V/cm electric field. This study serves to understand the electric field influence on the functional role of proteins.

Keywords: electric fields, field strength, energy input, enzyme dynamics, nonthermal processing

Introduction

The application of electric fields to biomaterials has advanced greatly in recent years, resulting in the formation of a new professional organization (International Society for Electroporation-Based Technologies and Treatments: ISEBTT) for the purpose of exploring these effects in detail. Applications abound in medicine (electrosurgery, electrochemotherapy), treatment of biocellulosic feedstocks for energy conversion, and the sterilization and pasteurization of foods. In typical treatments, operated in either batch or continuous-flow modes, the target material is placed between two electrodes and exposed to an electric field. The resultant ohmic heating principle is utilized for sterilization or pasteurization treatments in industry (1, 2). In addition to the thermal effect by ohmic heating, which generally employs alternating electric fields (50-60 Hz) of field strengths under 100 V/cm, the nonthermal effects of electric fields are also useful. Biological cell membranes have been found to become permeable, either reversibly (at low field strengths), or irreversibly (at higher field strengths). This phenomenon has been found useful in extraction of bioactive compounds, breakdown of cellulosic materials, and inactivation of microorganisms. While vegetative microorganisms are most affected, inactivation of some sporeformers has been noted as well (3, 4).

Growing experimental evidence has shown that electric fields cause biochemical changes, particularly in the range of the ohmic heating electric fields. This has led to the recent development of moderate electric field (MEF) processing technology that employs low-intensity electric fields, typically less than or equal to 1000 V/cm (5). In essence, the MEF processing takes the advantage of nonthermal effects of electric fields to control biochemical changes in

biological materials. Applications have included improved extraction of intracellular compounds, starch gelatinization, fermentation, and peeling of produce (1, 5). Nonthermal effects of moderate electric fields on a number of enzymes have been identified in several assay-based studies (6-13). In particular, the studies by Durham (10) and ourselves (11-13) have shown that the catalytic activity of enzymes can be enhanced or inhibited by manipulating the electric field strength, frequency, and treatment temperature.

In our previous studies with pectin methylesterase (PME), we developed rigid body dynamics models for translational and rotational motions of an enzyme molecule under electric fields (11, 12), which showed that electrophoretic translational motion results in enzymes behaving as if they were at a higher temperature than their surroundings (12). This would allow nonthermal activation at lower-than optimal activity temperatures and inactivation at higher-than optimal temperatures. Furthermore, models indicate the electric field-driven oscillatory and rotational motions of the enzyme molecule at lower electric field frequencies (11, 13) cause enhancements in activity upon change from oscillatory to rotational motion. However, a detailed understanding the experimental results requires an appreciation of the finer detail of the enzyme's protein structure that ultimately dictates its interaction with an external electric field.

At the simplest level of structure, a naturally occurring protein comprises nonpolar, polar, and electrically charged amino acid residues having different individual responses to an electric field. This non-uniformity represents different magnitudes of local flexibility and conformational dynamics within the molecule, which has been recognized as important for catalytic activity (14, 15). Molecular dynamics (MD) simulation is often the method of choice to

explore these internal motions and resulting conformational changes since such information is not accessible from experiment (16). A comprehensive review on the theory, computational algorithms, and their applications to modeling the effects of electromagnetic fields (EMFs) on various aqueous, nanoscale and biological systems has been reported (17). Studies investigating EMF effects by non-equilibrium molecular dynamics have identified different levels of EMF field strength responsible for structural changes and dynamics of amyloidogenic peptides and lysozyme (18, 19). Protein folding and unfolding dynamics at 300 K have been studied by molecular dynamics simulations with electric fields (EFs) applied as static fields and nanosecond pulsed fields (20-24). The results of these studies indicate high intensity electric fields ($> 10^8$ V/m) are necessary to observe significant denaturation effect during the simulation time frame (≤ 200 ns). Effects of electric fields on a peptide (chignolin) and a few protein structures have been previously investigated (25-29) using the GROMACS code. These studies were limited to less than 10 ns and, with respect to root mean square deviation, radius of gyration, dipole moment, solvent accessible surface area, and secondary structure analysis, they indicate the need for large electric field strengths (1 V/nm) and/or high temperatures (> 100 °C) for significant conformational changes (27-29).

PME is known as one of the most important enzymes found in plant-based biomaterials. Several experimental studies, including ours (11, 12), with applied electric field treatments on biomaterials have evidenced the role of nonthermal effects on PME activity. It is the aim of our present study to investigate the nonthermal effects of electric fields on the protein structure of PME, and thereby its catalytic function. By means of conventional molecular dynamics (MD) simulations performed at 50 °C, we capture electric field-driven internal motions and resulting

changes in the protein structure. We further examine fine molecular details at a practically applied electric field by running the simulations that are of far longer duration than in the previous studies. This simulation study demonstrates how electric fields interact with the PME structure at the molecular level, leading to intramolecular changes, consequently exerting nonthermal effects on catalytic activity.

Methodology

Molecular Dynamics (MD) simulations

All MD simulations were performed using GROMACS 5.1.2 software package (30) available on HPC clusters at the Ohio Supercomputer Center (Columbus, OH, USA). A detailed description of the molecular modeling procedure is available in the Supplementary Information (ESI). Electric field strength was varied on the basis of equivalent energy input described in the following section (**Table I**). Nonthermal effects were captured by running control simulations without electric field application at the same temperature, and comparing against simulations with electric fields.

Equivalent energy input

Generally, the time scale for MD simulations is limited to the nanosecond range, whereas electric field treatments operate at much longer time scales (seconds or minutes). Therefore, in order to utilize MD simulations to understand the molecular dynamics in realistic electric field treatments, the limited simulation times need to be accompanied with sufficiently large field strengths. In practice, simulation studies routinely use field strengths much larger (in the order of 1 V/nm) than those applied in either experimental or industrial settings (18, 19). We followed the same technique with normalization to total exposure under the condition of equivalent

energy in both types of treatments. Electric field treatments with the same energy input can be related as follows.

The fundamental equation governing the energy delivery in an electrical circuit can be written as (31):

$$Q = \frac{V^2}{R} t \quad (1)$$

where *Q* is energy (joules), *t* is time (seconds), *V* is voltage (volts), and *R* is resistance (ohms). In electric field treatments, the voltage in the above equation is expressed in terms of the electric field strength (*E*). For a given sample at a constant temperature (where R is constant), treatments having the same energy can be applied varying the field strength and the treatment time. Consequently, experimental and simulation treatments operate at the equivalent energy under isothermal conditions can be correlated as:

$$(E^2 t)_{exp} = (E^2 t)_{sim} \quad (2)$$

where the subscripts *exp* and *sim* stand for experimental and simulation, respectively. For a given experimental treatment, the above relationship allows choice of the simulation field strength and/or the time.

Justification

Since application of large simulation field strengths, while maintaining a constant temperature is not possible in experimental settings, we can only provide a theoretical justification for the equivalent energy input principle (Eq. 2). For this purpose, a series of

isothermal simulations were conducted at a constant E^2t, but at various field strength-time combinations. The change in atomic positions in response to the electric field exposure was determined by measuring the radius of gyration of the enzyme with respect to its center of mass. Triplicate simulations ($n=3$) were performed at each field strength-time combination and the measurements were time-averaged in each replicate. A one-factor analysis of variance (ANOVA) followed by Tukey's post hoc analysis were used to determine statistical significance ($P \leq 0.05$).

Enzyme dynamics influenced by electric field

Table I shows the experimental conditions tested. The test parameters included 50 °C temperature and 50 V/cm externally applied field strength. Previous experimental studies on tomato PME (11, 12) suggest enhanced sensitivity to electric fields when the enzyme is held at or near its optimal activity temperature, 65 °C. Consequently, at this sub-optimal test temperature (50 °C), the enzyme is present in its active form and is quite sensitive to electric fields. The selection of 50 V/cm field strength was arbitrary. However, this particular field strength is in the range of Moderate Electric Field (MEF) processing of foods and biological materials (5). Furthermore, the experimental study of tomato PME up to 10.5 V/cm (12) suggests the use of higher field strengths to increase nonthermal activation and inactivation effects. For a simulation time of 5 ns, the calculated simulation field strengths corresponding to five experimental treatment times are given in **Table I** (Eq. 2). It is important to note that the externally applied electric fields in this case are typically low-frequency (e.g. 50-60 Hz), sinusoidal, oscillating electric fields. However, the calculations by Eq. 2 use the amplitude of 50 V/cm root-mean-square (RMS) field strength, and given the short durations of MD simulations,

they effectively represent the effects of static electric fields. All these **Table I** simulations were carried out in triplicate (*n=3*) and the results are represented as average values. The replicate measurements were time-averaged and statistically analyzed, using a one-factor analysis of variance (ANOVA) followed by Tukey's post hoc analysis, to determine significant ($P \leq 0.05$) electric field effects.

Table I. MD simulation field strengths calculated on the basis of equivalent energy input for different experimental electric field treatments.

		Experimental		Simulation	
Exp. #	Temp. (°C)	*E* (V/cm)[a]	*t* (s)	*E* (V/nm)	*t* (ns)
(1)	50	50	5×10^{-9}	7.0710×10^{-6}	5
(2)	50	50	1/60	0.0129	5
(3)	50	50	30	0.5477	5
(4)	50	50	60	0.7746	5
(5)	50	50	100	1	5

[a] Root-mean-square voltage (sine wave) is shown. Amplitude (= sqrt (2) $\times$ 50) is 70.71 V.

One-microsecond MD simulations at 50 V/cm

Long-timescale MD simulations were run to explore PME's secondary structure, its hydrogen bond network, degree of hydration, and flexibility and conformational changes of the catalytic domain. The 50 V/cm simulation shown in Exp. # 1 (in **Table I**) was continued for 1 μs (1000 ns), and the results were assessed with respect to a similarly run control simulation without the external electric field (nofield). Details of the analyses are available in the Supporting Information. These simulations were triplicated (*n=3*) and the results are represented as average values. Time-averaged data were employed to determine the statistical significance ($P \leq 0.05$) and to calculate the relative change, expressed as a percentage (%) with respect to the nofield control, in the presence of the 50 V/cm electric field.

Results and Discussion

Application of electric fields and temperature control

External electric fields do work on the system under study, consequently, increasing its temperature. In experimental studies on the nonthermal effects, temperature is generally controlled by simultaneously cooling the system while applying electric fields (3, 4, 6-11, 13). We followed the same method in this simulation study to observe the nonthermal effects. This was accomplished by thermostatting the simulation system (50 °C) to absorb the heat generated by the electric fields. We want to note that similar isothermal molecular dynamics simulations with applied electric fields are available in the literature (25-29).

Furthermore, we calculated the amount of (ohmic) heat generation and the temperature rise under the simulation field strengths and the time scale in **Table I**, for an aqueous medium with the properties of water (typical of such systems). The calculations ensure that due to low electrical conductivity the ohmic heating is limited and can be controlled by providing adequate cooling using an external heat exchanger, as in the experimental studies.

Theoretical validity of the equivalent energy input principle

In electric field simulations, the electrophoretic driving force (=$q_i E(t)$) is applied to each partial charge i , with charge value q_i. Then, Newton's equation of motion becomes (17,18):

$$m_i \ddot{r}_i = f_i + q_i E(t) \quad (3)$$

where f_i is the force exerted by the applied force field. The m_i is the mass of atom i with the charge value q_i and $\ddot{r}_i = \frac{d^2 r_i}{dt^2}$. Solving the above equation (Eq. 3) yields displacement (r_i) in the atomic position during exposure to the electric field. In this validation study, we used the radius of gyration (R_g) since it measures distance of atoms from the center of the molecule (32). The change in the R_g measurement therefore directly relates to the displacement of atoms under the influence of electric field. Furthermore, the R_g value describes the level of compactness providing insights into the overall dimensions of the molecular structure (28, 33).

Table II shows the constant E^2t simulations conducted at 50 °C. The resulting R_g measurements indicate that, above a simulation time of 5 ns, the change in the overall structural dimensions of the enzyme molecule is only 1% and not statistically significant ($P >$

0.05). Consequently, it is evident that the electric field treatments with the same energy input at a given temperature cause comparable effects on the overall protein structure. As can be seen in **Table II**, the same amount of energy can be applied as either larger field strengths and shorter treatment times or smaller field strengths and longer treatment times. Therefore, our validation study supports the use of the equivalent energy input principle to correlate experimental and simulation conditions.

Table II. The simulation tests and their (mass-weighted) R_g measurements for the validation of the equivalent energy input principle. All these tests were conducted at 50 °C. The field strength-time combination of 0.5477 V/nm for 5 ns is the same simulation setting used in the Exp. # 3 in **Table I**. Numbers in parentheses indicate standard deviations of mean (*n=3*) R_g values. Percentage (%) retention in the R_g value is calculated with respect to that at the 0.5477 V/nm for 5 ns simulation.

E (V/nm)	*t* (ns)	E^2t (V^2.ns/nm^2)	*Rg* (nm)	% Retention
0.5477	5	1.50	1.9566[a] (0.0135)	100
0.2449	25	1.50	1.9408[a] (0.0059)	99
0.1732	50	1.50	1.9426[a] (0.0017)	99
0.1095	125	1.50	1.9382[a] (0.0024)	99
0.05477	500	1.50	1.9438[a] (0.0061)	99

[a] Mean R_g values with the same superscript letter are not significantly different ($P > 0.05$).

Structural fluctuations

It has long been known that proteins have a rather fluid, dynamic structure with rapid conformational fluctuations (34). The reality of this structural flexibility is further evident in the Protein Data Bank (PDB) structure database, which includes not only a set of fixed coordinates but also, among other factors, the temperature B factors to denote the protein's thermal fluctuations (35). For the selected PDB structure of PME (PDB ID: 1gq8), we herein examined structural fluctuations driven by electric fields.

The enzyme has 319 amino acid residues and their fluctuations with and without electric field applications (50 °C) are shown in Fig. 1 A. It may be seen that thermal fluctuations of the residues occurring in the absence of the electric field (nofield) are increased significantly by applying electric fields of higher field strengths (corresponding to longer experimental treatment times, **Table I**, using the equivalent energy input principle). Moreover, at lower field strengths, equivalent to 5 ns and 1/60 s treatment times (**Table I**), the electric field-driven fluctuations closely follow the thermal fluctuation profile of the residues with some noticeable peaks and dips. All the above changes in fluctuation with applied electric fields are purely nonthermal and clearly show the efficacy of electric field treatment on protein structure. By zooming in to the fine details of the RMSF curve of 5 ns, we examined the nonthermal fluctuation of the residues at 50 V/cm (Exp. # 1, **Table I**). Fig. 1 B shows % RMSF values calculated for each residue with respect to its thermal-only (nofield) fluctuation. The labeled residues have statistically significant ($P \leq 0.05$) percentage fluctuations and reveal interesting information about internal motions in the molecule. Evidently, the residues exhibiting fluctuation peaks are polar and electrically charged, whereas the fluctuation dips correspond to

nonpolar (hydrophobic) residues. It is also seen that these peaks and dips are not quite isolated indicating that the surrounding residues also respond to electric field in the same manner. This pattern represents the occurrence of simultaneous expansion (pull) and contraction (push) motions in different parts of the protein structure under the 50 V/cm electric field. Such electric field-driven conformational fluctuations open up the protein's core, as visualized in Movie S1 (ESI) showing exposure of a sulfur atom (in a Cys or Met residue) in the hydrophobic interior at 2 to 5 s. In contrast, Movie S2 (ESI) illustrates the thermal-only (nofield) fluctuations, which are evidently limited to the surface atoms.

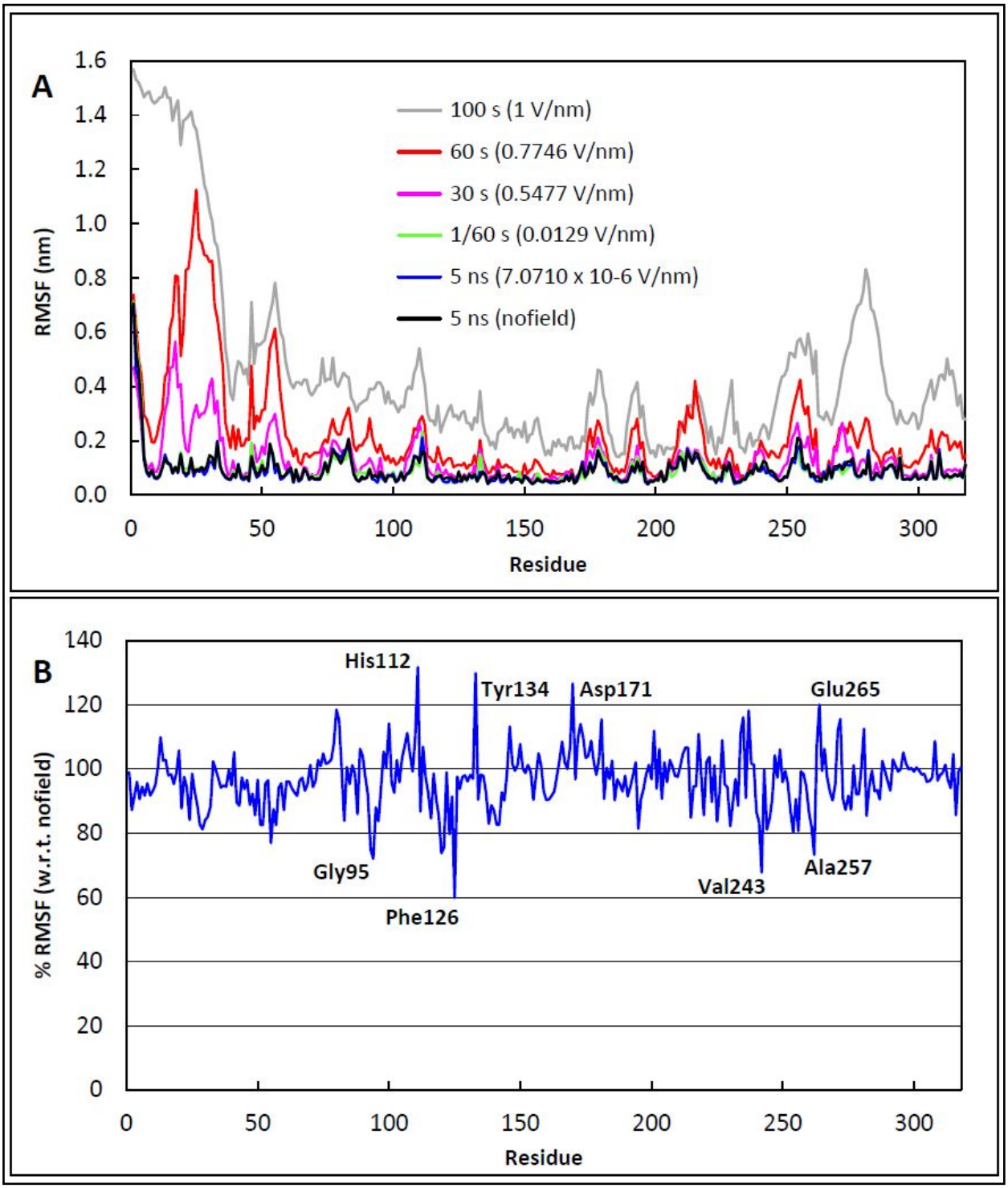
A
RMSF (nm)
Residue
100 s (1 V/nm)
60 s (0.7746 V/nm)
30 s (0.5477 V/nm)
1/60 s (0.0129 V/nm)
5 ns (7.0710 x 10-6 V/nm)
5 ns (nofield)
B
% RMSF (w.r.t. nofield)
Residue
His112
Tyr134
Asp171
Glu265
Gly95
Phe126
Val243
Ala257

Figure 1. (A) Average root-mean-square fluctuation (RMSF) of the enzyme residues for different electric field treatments (**Table I**). The 50 V/cm experimental treatment times and the corresponding simulation field strengths (in parentheses) are represented in different colors. (B) Percent (%, w.r.t. nofield) RMSF of the residues during the 50 V/cm simulation for 5 ns (i.e., Exp. # 1, **Table I**). The peaks and dips, labeled with respective residue labels, show statistically significant ($P \leq 0.05$) percentage fluctuations.

Conformational changes

As a consequence of the above localized conformational fluctuations, changes to the global protein conformation are to be expected, potentially impacting the enzyme's functional role. To explore the degree of change in conformation, root-mean-square deviation (RMSD) values of the enzyme molecule were recorded under the electric fields (Fig. 2 A). It is clearly seen that the higher the field strength (≥ 0.5477 V/nm or when the treatment time ≥ 30 s, **Table I**), the greater the RMSD value. The statistical analysis of time-averaged measurements shows that the RMSD values at and above 0.5477 V/nm are significantly different ($P \leq 0.05$) from each other and from those below this field strength. The large RMSD values at higher field strengths (≥ 0.5477 V/nm) correspond well with the high amplitude fluctuations of flexible residues (Fig. 1 A) and indicate heavily disrupted protein conformation under those electric fields (36). Contrary to the above pattern, Fig. 2 A further shows a minor ($P > 0.05$) reduction of nofield RMSD by the electric fields of lower field strengths, equivalent to 5 ns and 1/60 s treatment times (**Table I**). Due to the proximity of these RMSD curves, we compared their RSMD distributions plotted as shown in Fig. 2 B. As can be seen, the RMSD distribution of nofield is shifted progressively to the left by the electric fields corresponding to the 5 ns and 1/60 s treatment times. This reduction of RMSD of the protein structure suggests that the enzyme undergoes lesser conformational change at these lower field strengths compared to the thermal-only treatment. Such RMSD reductions during protein MD simulations influenced by the electric fields at specific temperatures have been already reported in the literature (29). The RMSD distributions in Fig. 2 B further reveal that, during shorter exposure times such as 5 ns, PME's protein structure can withstand electric fields as high as 0.0129 V/nm (= 129 kV/cm) without

undergoing significant conformational changes. This apparent stability of the protein conformation suggests the need of longer treatment (exposure) times for inactivating enzymes at lower field strengths. Additionally, this inactivation effect can be fine-tuned with the test temperature, as evident from our previous experimental study (12).

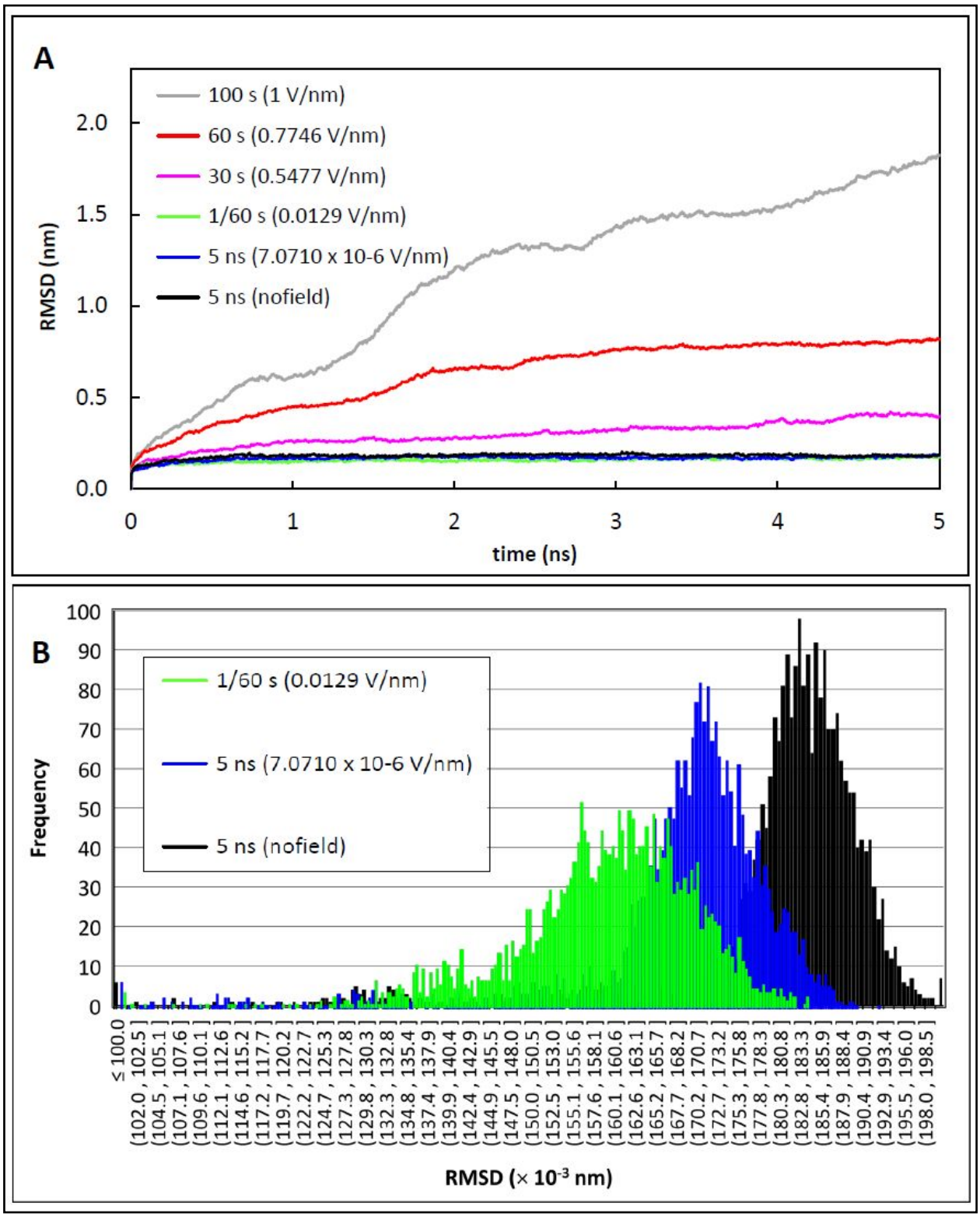
A
100 s (1 V/nm)
60 s (0.7746 V/nm)
30 s (0.5477 V/nm)
1/60 s (0.0129 V/nm)
5 ns (7.0710 x 10-6 V/nm)
5 ns (nofield)
RMSD (nm)
time (ns)
B
1/60 s (0.0129 V/nm)
5 ns (7.0710 x 10-6 V/nm)
5 ns (nofield)
Frequency
RMSD (× 10-3 nm)

Figure 2. (A) Time evolution of average RMSD values of the enzyme molecule for the different MD simulations shown in **Table I**. The 50 V/cm experimental treatment times and the corresponding simulation field strengths (in parentheses) are represented in different colors. (B) The RMSD value (in $\times 10^{-3}$ nm) distribution histograms for the 5 ns (7.0710×10^{-6} V/nm) and 1/60 s (0.0129 V/nm) electrical treatments and the nofield treatment.

Changes in structural properties and electrophoretic motion

The RMSD analysis indicates varying degree of conformational changes depending on the field strength, or in other words, the treatment time (**Table I**). To further assess the electric field effects on the PME's protein structure, radius of gyration (R_g) and solvent accessible surface area (SASA) measurements were carried out under the electric fields.

The R_g values of the enzyme molecule with respect to its center of mass under the electric fields are shown in Fig. 3 A. As can be seen clearly, the 0.7746 and 1 V/nm electric fields (corresponding to 60 and 100 s treatment times, **Table I**) largely elevate the original (nofield) R_g of the enzyme indicating reduced compactness of atomic packing in the molecular structure. The time-averaged measurements show that the R_g values at these two field strengths are significantly different ($P \leq 0.05$) from the rest of the R_g values at low-intensity electric field and nofield treatments. The statistical analysis further shows that the differences in R_g values at these two field strengths (0.7746 and 1 V/nm) are significantly different ($P \leq 0.05$) from each other. A similar trend with the same statistical information can be found in the SASA curves (Fig. 3 B), supporting the loose structural packing (i.e. spread of the structure) as evidenced by the R_g values. More precisely, with the expansion of molecular structure under high-intensity electric fields, the surface area available for solvent accessibility increases as indicated by the SASA curves. Therefore, from the increased R_g and SASA values influenced by these electric fields, it is possible to deduce the change in catalytic activity due to unfolded protein structure. On the other hand, the R_g and SASA plots in Fig. 3 further show only minimal ($P > 0.05$) changes to the original (nofield) R_g and SASA values at low-intensity field strengths, equivalent to 5 ns and 1/60 s treatment times (**Table I**). It is found that these low-intensity electric fields in fact

result in a slight reduction in the nofield R_g value and that is quite visible for the 1/60 s treatment time. Moreover, the time-averaged SASA measurements assert only a minor change (below 1%) to the nofield SASA value under these low-intensity electric fields. The above evidence therefore indicates that the global topology of the protein structure is preserved in the presence of the electric fields of lower strengths.

The varying R_g values in Fig. 3 A also correspond to the changes in moment of inertia (I) of the molecule and consequently its rotational motion under the electric fields. From classical mechanics, electrophoretic driving force for rotational motion of a molecule can be described by Eqs. 4-6 (11-13).

The torque ($\boldsymbol{\tau}_e$) exerted by an electric field (E) on a dipole (μ) is given by:

$$\boldsymbol{\tau}_e = \boldsymbol{\mu} \times \boldsymbol{E} \tag{4}$$

In accordance with laws of motion, the angular velocity (ω) for different orientations can be written as:

$$I\frac{d\boldsymbol{\omega}}{dt} = \boldsymbol{\mu} \times \boldsymbol{E} \tag{5}$$

The relation for angular displacement (θ) is then found by:

$$I\frac{d^2\boldsymbol{\theta}}{dt^2} = \boldsymbol{\mu} \times \boldsymbol{E} \tag{6}$$

At each simulation field strength (**Table I**), dipole moment of the PME molecule was obtained by the MD simulations. Moment of inertia of the molecule was calculated by the R_g data in Fig. 3 A using the following relation (Eq. 7), where m is the mass of the molecule.

$$R_{\mathrm{g}} = \sqrt{\frac{I}{m}} \tag{7}$$

Fig. S1 (ESI) shows these structural data, which reveal not only the moment of inertia but also the dipole moment of the molecule is subjected to change under the electric fields. To gain insight into the rotational motion, the data in Fig. S1 were time-averaged (Fig. S2, ESI) and evaluated for their change according to Eq. 6.

For a given orientation to the electric field, the torque ($\boldsymbol{\mu} \times \boldsymbol{E}$) experienced by the molecule is increased due to both the dipole moment and the electric field increase, when the field strength is above 0.0129 V/nm (Fig. S2). Moreover, at these electric fields, Fig. S2 also shows an increase of (mass) moment of inertia of the molecule with increasing field strength. However, it can be seen that the average dipole moment increase is significantly greater ($P \leq 0.05$) than the average increase of inertia, thus suggesting a high tendency to rotational motion of the molecule under these electric fields. Even at relatively low field strengths, 7.0710×10^{-6} and 0.0129 V/nm, the data in Fig. S2 depict a trend in rising dipole moment with declining inertia, consequently leading to rotational motion.

In addition, we examined the translational motion via MD simulation measurements of mean square displacement (MSD) of the enzyme's center of mass under these electric fields (Fig. S3, ESI). As seen from the figure, the MSD as a function of time exhibits two distinct regimes of behavior. At higher field strengths above 0.0129 V/nm, the electric fields result in significantly large ($P \leq 0.05$) MSD values that increase with increasing field strength. This increasing trend is consistent with the direct correlation between electrophoretic driving force for translational motion and field strength that we reported in our previous studies (11-13).

However, at relatively low field strengths such as 7.0710×10^{-6} and 0.0129 V/nm, the MSD values are comparatively very small and insignificant ($P > 0.05$), even become less than the nofield MSD values (i.e. Brownian displacement). The reduced MSD values may indicate insufficient electrophoretic driving force (translational) produced by these lower field strengths to overcome the other local environmental forces on the molecule (11-13).

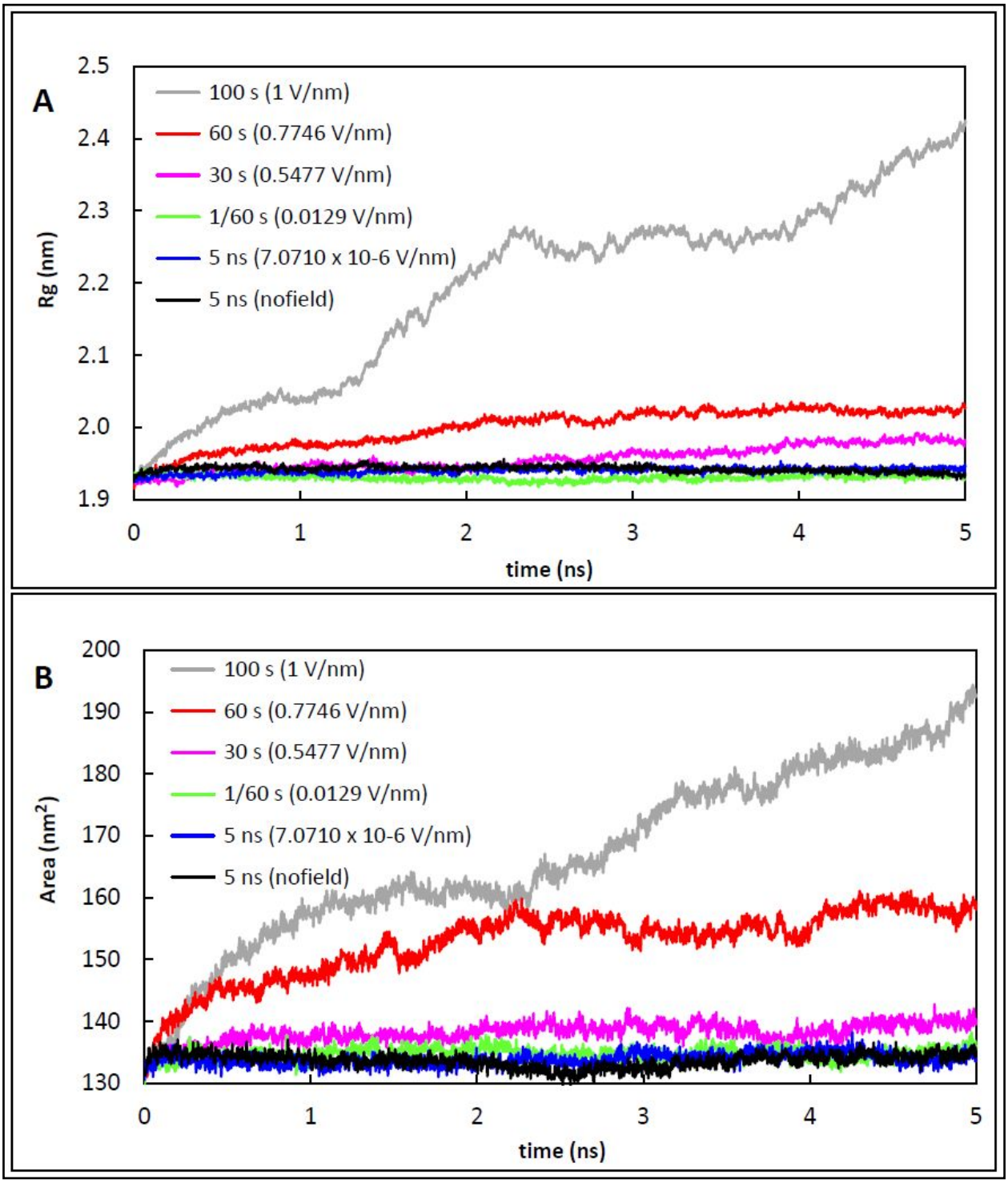
A
Rg (nm)
2.5
2.4
2.3
2.2
2.1
2.0
1.9
0
1
2
3
4
5
time (ns)
100 s (1 V/nm)
60 s (0.7746 V/nm)
30 s (0.5477 V/nm)
1/60 s (0.0129 V/nm)
5 ns (7.0710 x 10-6 V/nm)
5 ns (nofield)
B
Area (nm2)
200
190
180
170
160
150
140
130
0
1
2
3
4
5
time (ns)
100 s (1 V/nm)
60 s (0.7746 V/nm)
30 s (0.5477 V/nm)
1/60 s (0.0129 V/nm)
5 ns (7.0710 x 10-6 V/nm)
5 ns (nofield)

Figure 3. Time evolution of average radius of gyration, R_g (A), and solvent accessible surface area, SASA (B) of the enzyme molecule for different electric field treatments (**Table I**). The 50 V/cm experimental treatment times and the corresponding simulation field strengths (in parentheses) are represented in different colors.

More molecular details revealing nonthermal effects of 50 V/cm electric field

As described in the introduction, moderate electric field processing technologies employ relatively lower field strengths (5). Under such electric fields, a number of assay-based studies, including ours on PME and α-amylase, have identified nonthermal effects on the catalytic activity (6-13). To gain further insights into the catalytic activity under the practically applied electric fields, we continued to investigate fine molecular details of PME at the 50 V/cm electric field (Exp. # 1, **Table I**) for a longer timespan (1 μs). Some of our results are statistically significant at the 0.05 level.

Flexibility and conformational changes in the catalytic domain

Numerous studies in the literature have revealed that there is a correlation between active site rigidity and catalytic activity of enzymes. Johansson et al. have recognized both the pectin binding site residues (Phe84, Tyr139, Phe160, Tyr222, Trp227, Phe250, Trp252) and the active site residues (Gln113, Gln135, Asp136, Asp157) responsible for PME's catalytic activity (37). For these residues in the enzyme's catalytic domain (Fig. 4), we measured the B factor values of C-alpha carbon atoms in the presence and absence of the electric field. Using the B factor values, relative B factor (%, w.r.t. nofield) was calculated for each residue to determine its flexibility under the electric field (Fig. 5). As seen in the figure, a majority of both pectin binding and active site residues attain a relative B factor above 100% in the beginning of the electric field application (0-200 ns). This indicates the enzyme's catalytic domain indeed "senses" and becomes more flexible upon application of the field. However, it is also seen that the above

fluctuating residues overcome the electric field disturbance and lose this flexibility, becoming rigid, with prolonged exposure to the field (800-1000 ns). Noticeably, Fig. 5 B indicates a considerably (not significant) elevated rigidity of the Asp157 residue in the active site. This residue is known to initiate the mechanism of enzymatic hydrolysis of pectin acting as the nucleophile (37). Moreover, compared to the other residues in the active site, Asp157 is located closer to the enzyme surface (37), and therefore better exposed to the electric field, consequently exhibiting an elevated rigidity. In general, increased rigidity of the active site implies enhanced kinetic stability, in other words, slower enzymatic reaction (38).

We performed some simulation measurements to understand physical changes in the catalytic domain under the electric field (**Table III**). The volume measurement shows that a significant ($P \leq 0.05$) reduction in volume of the catalytic domain by 28 $Å^3$ under the electric field. This suggests shrinking of the catalytic domain that may lead to inhibition of the catalytic activity. Shrinkage is further supported by the reduction in the distance (by 0.4 Å, $P > 0.05$) between pectin binding and active site regions. The changes in the active site interresidue distances indicate altered, or possibly reduced, cavity size under the electric field. Moreover, we used Ramachandran plots to assess stereochemical changes in the catalytic domain residues. The relevant Ramachandran plots for the simulated molecule are shown in Fig. S4 (ESI). MolProbity software was employed for the Ramachandran plot calculations, which checks the detailed residue-by-residue stereochemical quality of protein structure (39). These residue-specific data for the catalytic domain are shown in **Table III**. It appears that the electric field does not result in any unfavorable steric changes to the pectin binding site residues. However, Gln113 and Asp157 residues in the active site are subjected to Ramachandran deviations under

the electric field. This indicates the ϕ-ψ torsion angles of these two residues are changed by the electric field and such changes would cause steric hindrances in the active site. The large Cβ deviations (> 0.25 *Å*) of these two residues also indicate severe bond angle distortions and geometrical changes (40). With all these changes, the active site may be sterically incompatible for the enzymatic reaction to proceed under the electric field.

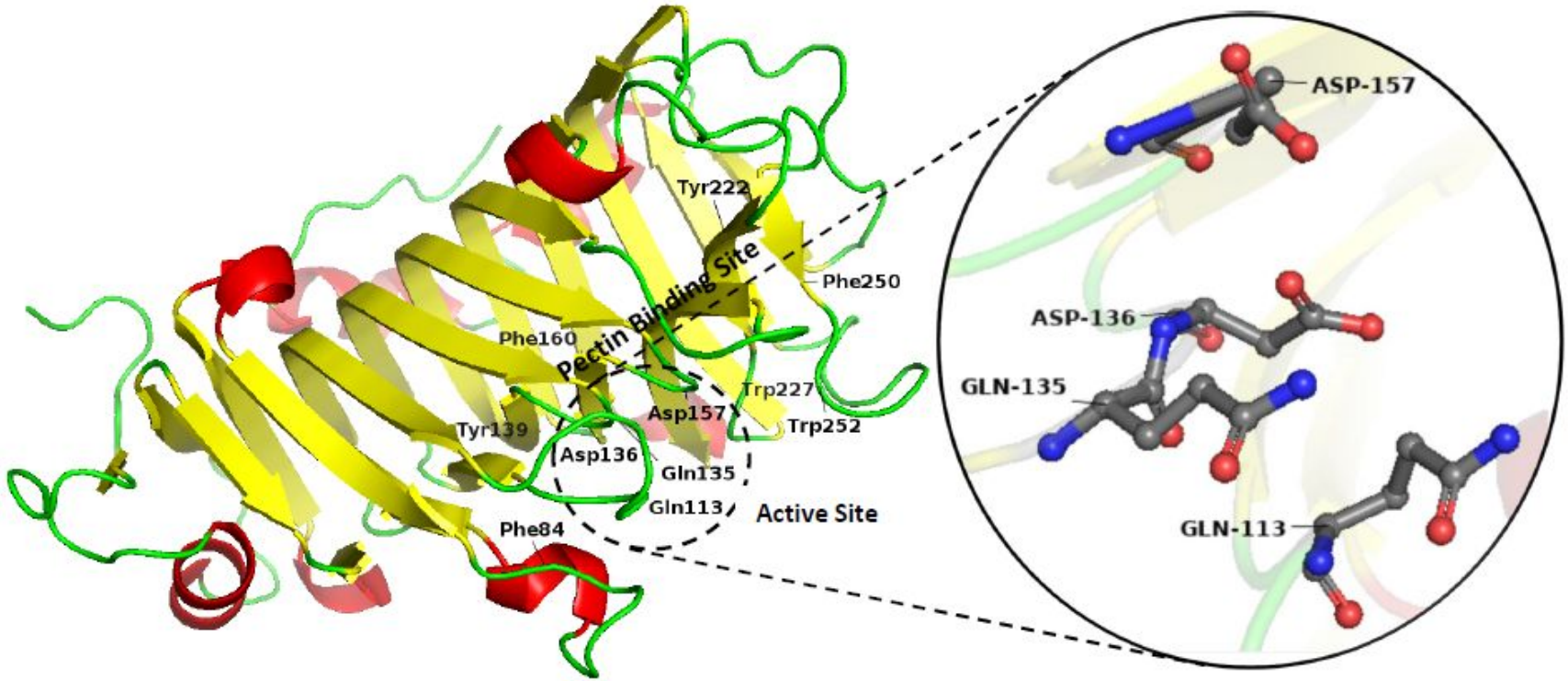

Figure 4. The x-ray crystallographic structure of PME enzyme (PDB ID: 1gq8) showing its residues in the catalytic domain. The pectin binding site spreads across the molecule and the insert shows enlarged view of the active site residues involve in the catalytic conversion. They function as: Asp157, nucleophile that initiates the attack on pectin; Asp136, acid/base that involves in releasing methanol; Gln113 and Gln135, form an anion hole to stabilize the transition state (37).

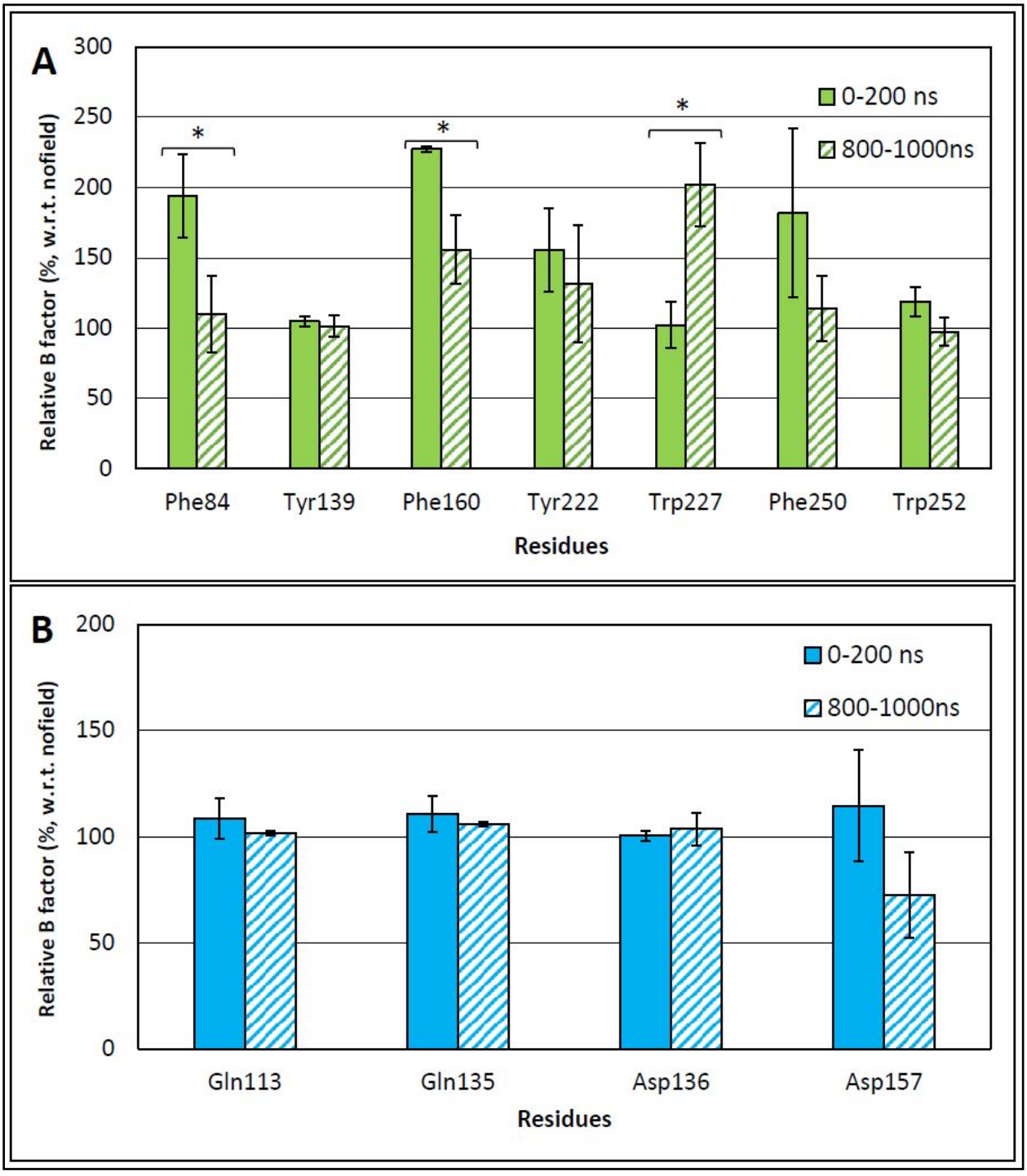
A
300
250
200
150
100
50
0
Relative B factor (%, w.r.t. nofield)
0-200 ns
800-1000ns
*
*
*
Phe84
Tyr139
Phe160
Tyr222
Trp227
Phe250
Trp252
Residues
B
200
150
100
50
0
Relative B factor (%, w.r.t. nofield)
0-200 ns
800-1000ns
Gln113
Gln135
Asp136
Asp157
Residues

Figure 5. Relative B factors for the pectin binding (A), and active site (B) residues in the presence of the 50 V/cm electric field. Two bars for each residue display the first (0-200 ns) and the last (800-1000 ns) stages of the simulation. For each residue for each time frame, relative B factor was calculated by means of the average B factor values from the electric field and nofield treatments. Error bars show percentage standard deviations, and significantly different ($P \leq 0.05$) pairs are indicated with asterisks.

Table III. Some simulation measurements to describe the electric field influence on enzyme's catalytic domain. The quantitative data were averaged over the course of 1 μs simulation. The standard deviation of the mean (*n=3*) is shown in the parentheses.

Measurement	Nofield (50 °C)	Electric field (50 V/cm, 50 °C)	change (w.r.t. nofield)
Volume [a] (*Å³*)	3640 (4)	3612 (4)	- 28
Distances [b] (nm)			
Active site - Binding site	0.48 (0.01)	0.44 (0.03)	- 0.04
Asp136 - Asp157	2.89 (0.01)	2.86 (0.04)	- 0.03
Gln113 - Gln135	2.81 (0.01)	2.82 (0.01)	+ 0.01
Ramachandran analysis [c] (residue-by-residue)			
All binding site residues	favored	favored	
Gln113	favored	**outlier**, Cβ deviation: 0.43 *Å*	
Gln135	favored	favored	
Asp136	favored	favored	
Asp157	favored	**allowed**, Cβ deviation: 0.46 *Å*	

[a] combined volume of both pectin binding and active site regions. The difference between the means is statistically significant ($P \leq 0.05$).

[b] center-of-mass distances.

[c] performed by using MolProbity software (39). Trajectory file of the molecule at the end of each MD simulation was used for the analysis. Ramachandran deviations are shown in bold fonts with their Cβ deviations. For all the Ramachandran favored residues, the Cβ deviations are below 0.25 *Å*.

Dynamics of water around the enzyme surface

It is believed that water plays a primary role in determining the structural stability and biological function of proteins (41). Both experimental and simulation studies have indicated that water present near the protein surface is dynamically coupled to the protein itself and that surface hydration water (i.e., biological water) exhibits different properties than the water in the pure bulk state (41-43). The dynamical response of water is intimately connected with the lifetime of hydrogen bonds. It is considered that the hydrogen bonds between the protein molecule and the water present in its hydration layer have a long lifetime (41). Using the theory of reactive flux dynamics by Luzar and Chandler (41, 43), we examined the electric field's influence on the lifetime of the interfacial hydrogen bonds (**Table IV**). It is clear from the data that the electric field significantly reduces ($P \leq 0.05$) the lifetime of the hydrogen bonds between the enzyme and its hydration water molecules. It can also be seen that the magnitude of this electric field effect increases with continued exposure to the electric field. The breaking and forming of hydrogen bonds is known as a dynamic process taking place at the protein-water interface (41) and, from our data, it appears that the electric field interferes with the kinetics of hydrogen bonds. The shorter lifetime of the enzyme-water hydrogen bonds further indicates the lower degree of rigidity of the enzyme's hydration layer under the electric field.

Table IV. Influence of electric field on the enzyme-water hydrogen bond lifetime. The values are average reactive flux hydrogen bond lifetimes (in ps) calculated according to the Luzar and Chandler's theory (41, 43). Numbers in parentheses indicate standard deviations of triplicate (*n=3*) measurements.

Simulation time	Nofield	Electric field (50 V/cm)	% change (w.r.t. nofield)
Up to 100 ns	134[a] (11)	112[b] (4)	- 16
100 – 1000 ns	263[a] (58)	162[b] (21)	- 38

[a, b] In the same row, mean values with different superscript letters differ significantly ($P \leq 0.05$).

Secondary structure propensity

We employed the Define Secondary Structure of Proteins (DSSP) algorithm to compute the secondary structural elements in PME. The data were then used to calculate the retention of each element in the presence of 50 V/cm electric field, as shown in **Table V**. As can be seen, there is a noticeable reduction in the helical content, including about a 10% drop in the α-helix elements, in the presence of the electric field. Moreover, it appears that the contents of some structural elements, such as bends, β-sheets, and turns, are increased by the electric field. The data in **Table V** therefore imply unwinding of helices and transformation into the other forms of secondary structure under the influence of the electric field. Interestingly, in the literature, enzyme inactivation studied by circular dichroism (CD spectra) has shown that loss of α-helix content, while increasing the contents of β-sheet, turn and unordered structural elements, are associated with the inactivation of horseradish peroxidase (44), lysozyme (45), and polyphenoloxidase (46). Conversely, another study by CD spectral analysis has shown an increase in α-helix content along with a reduction in random coil content relate to the activation effect of α-amylase (47).

Furthermore, the stability of helices is known to involve interactions with salt bridges in protein structures (48). We investigated if there is a change in the number of salt bridges with the reduction in helical content (**Table V).** Using the VMD Salt Bridges Plugin, the number of salt bridges was measured in the trajectories of the enzyme subjected to the electric field and nofield treatments. However, we found that the total salt bridge count in both treatments was nearly the same (17 ± 1). This finding further indicates that the salt bridges (i.e., ionic interactions) are unaffected by the 50 V/cm electric field.

Table V. Relative percentage (%, w.r.t. nofield) of secondary structure elements in the presence of 50 V/cm electric field.[a]

Str [b]	Coil	β-Sheet	β-Bridge	Bend	Turn	α-Helix	5-Helix	3-Helix
100.0	98.1	101.5	89.6	104.3	103.2	90.1	68.0	89.9

[a] The relative percentage of each secondary structure element was calculated by employing average populations under the electric field and nofield treatments. Differences between these populations are not statistically significant at the 0.05 level.

[b] Structure = α-Helix + β-Sheet + β-Bridge + Turn.

Hydrogen bond analysis

We examined the electric field influence on both intra- and intermolecular hydrogen bonds in the presence of a 50 V/cm electric field (Figs. 6 A and 6 B). The hydrogen bond analysis includes averaging the number of bonds over 100 ns time frames (Figs. 6 C and 6 D) followed by calculation of relative percentages w.r.t. nofield (Fig. 6 E). While the data not significant at the 0.05 level, there are some noticeable changes in the hydrogen bonds, warranting further discussion.

The Fig. 6 E indicates that, upon application of the electric field (particularly up to 100 ns), more intramolecular hydrogen bonds are retained in the enzyme molecule compared to that in the nofield treatment. However, with continued electric field application, the enzyme keeps losing its internal hydrogen bonds relative to the nofield treatment. These phenomena may be explained by the higher diffusion of surrounding water molecules, relative to the enzyme structure, allowing the enzyme to form more internal hydrogen bonds upon electric field application. This pattern changes with the continued exposure as the enzyme begins to respond to the electric field exposing its structure (i.e., unfolding). In line with the above explanation, the change in intermolecular hydrogen bonds between the enzyme and surrounding water follows exactly the opposite trend, exhibiting a smaller number of enzyme-water hydrogen bonds under the electric field up to 100 ns, and thereafter increased hydrogen bond formation with prolonged exposure to the electric field. Therefore, from the two complementary graphs in Fig. 6 E, it is evident that the 50 V/cm electric field: ***(i)*** stabilizes the enzyme's secondary structure preserving the network of intramolecular hydrogen bonds for a short duration (approximately up to 100 ns); ***(ii)*** perturbs the secondary structure by breaking the

intramolecular hydrogen bonds with prolonged exposure. It should be noted that experimental (CD and fluorescence spectroscopic) evidence does exist for unfolding of lysozyme and BSA proteins with prolonged exposure to electric fields, even as low as 5 V/cm and below 25 °C (45).

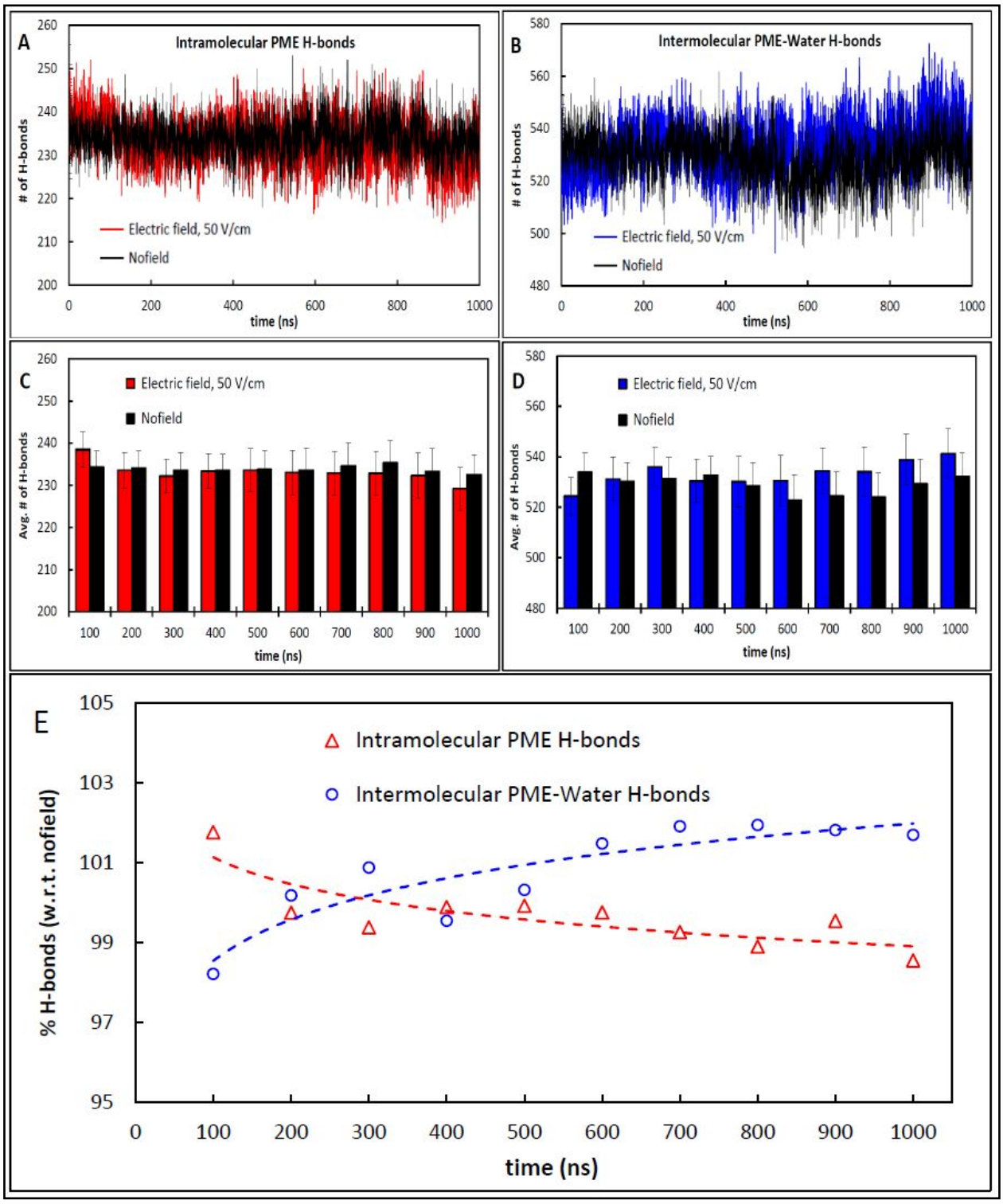
A
Intramolecular PME H-bonds
# of H-bonds
time (ns)
Electric field, 50 V/cm
Nofield
B
Intermolecular PME-Water H-bonds
# of H-bonds
time (ns)
Electric field, 50 V/cm
Nofield
C
Electric field, 50 V/cm
Nofield
Avg. # of H-bonds
time (ns)
D
Electric field, 50 V/cm
Nofield
Avg. # of H-bonds
time (ns)
E
Intramolecular PME H-bonds
Intermolecular PME-Water H-bonds
% H-bonds (w.r.t. nofield)
time (ns)

Figure 6. Electric field influence on the number of hydrogen bonds. Time evolution of intramolecular hydrogen bonds within the enzyme (A), and intermolecular hydrogen bonds between the enzyme and the surrounding water (B). (C) and (D) represent the respective average number of hydrogen bonds in each 100 ns time frame. The error bars represent standard deviation of the averaged values. (E) Relative change (%, w.r.t. nofield) of each type of hydrogen bonds under the influence of 50 V/cm electric field. The percentages were calculated using the averaged data (in C and D), and the error bars are not shown for clarity.

Hydration of the enzyme

The degree of hydration is expected to vary with protein folding and unfolding events (49). Given the importance of surface hydration water, as we described in a preceding section, the number of water molecules in the enzyme's hydration shell (5 *Å* thickness) were measured with and without electric field application. The results in Fig. S5 (ESI) indicate slightly reduced ($P > 0.05$) enzyme hydration shortly after the electric field is applied. This reduced hydration shell density, upon application of the electric field, was previously described as higher diffusion of the surrounding water relative to the enzyme molecule. However, with continued exposure to the electric field, the degree of hydration tends to increase ($P > 0.05$) forming more intermolecular hydrogen bonds with water. Moreover, this increase of hydration shell density implies higher electrostriction pressure and stronger local electric field (produced by water dipoles) acting on the enzyme molecule (50).

Finally, in contrary to the catalytic inhibitory effect of the electric field, we evidenced nonthermal activation of tomato PME up to 70 °C when subjected to 60 Hz oscillating electric fields (12). This particular study, however, was conducted at much lower field strengths (below 10.5 V/cm) besides the oscillating (sine wave) electric field. In fact, the activation of biological processes under such low-intensity electric fields is widely known and those electric fields are used with a frequency control when the stimulation effect is undesired (51). In this line, our simulation results at 50 V/cm (50 °C) may provide valuable information for controlling the field strength to achieve inhibited catalytic activity under electric fields.

Conclusions

In this work, we show evidence of nonthermal effects exerted by electric fields on PME's protein structure, resulting in internal motions in some local regions and conformational changes in the whole molecule and its catalytic domain. It is also seen that the magnitude of these nonthermal effects has strong field strength and treatment time dependence and that, consequently, can be used as a tool to manipulate the efficacy of electric field.

By studying the molecular dynamics at 50 V/cm for a relatively long timespan (1 μs), we unveil the fine molecular details of PME influenced by the electric field. Our results show significant ($P \leq 0.05$) reductions in the size of the catalytic domain and in the enzyme-water hydrogen bond lifetime under the influence of 50 V/cm electric field. The results also highlight the electric field sensitivity of the enzyme's secondary structure and the hydrogen bonds, providing insights into enzymatic reaction rates under electric fields. The nonsignificant effects are likely due to the low applied field strength, and those effects might become significant at longer timespans ($>$ 1 μs), as evidenced by the experimental data.

Since these simulations represent *in-silico* measurement, an important question is whether or not these electric field influenced structural changes are retained after the field is removed. We assume the answer depends on the severity of the electric field treatment at a given temperature. Furthermore, electric field frequency is also known to play a role in enzyme catalyzed reactions. Nevertheless, our study provides detailed information about specific electric field interactions at the molecular level of enzymes.

Conflicts of Interest

There are no conflicts to declare.

Acknowledgments

Support of USDA-NIFA-AFRI Grant No 2017-67017-26471 is gratefully acknowledged. Salaries and research support provided by the College of Food Agricultural and Environmental Sciences, The Ohio State University via the USDA NIFA NC-1023 Regional Research Project*: Engineering for Food Safety and Quality*. References to commercial products and trade names is made with the understanding that no endorsement or discrimination by The Ohio State University is implied. Simulations using GROMACS were performed with support from the Ohio Supercomputer Center Project PAS0587.

References

1. S. K. Sastry, in Ohmic Heating in Food Processing, edited by H. S. Ramaswamy, M. Marcotte, S. Sastry, K. Abdelrahim (CRC Press, Boca Raton, FL, 2014), pp 3-6.

2. N. Kaur, and A. K. Singh, Crit. Rev. Food Sci. Nutr., 2016, 56, 2338.

3. R. Somavat, H. M. H. Mohamed, Y-K. Chung, A. E. Yousef, and S. K. Sastry, J. Food Eng., 2012, 108, 69.

4. R. Somavat, R., H. M. H. Mohamed, and S.K. Sastry, LWT – Food Science and Technology, 2013, 54, 194.

5. S. K. Sastry, Food Science and Technology International (FSTI), 2008, 14 (5), 419.

6. I. Castro, B. Macedo, J. A. Teixeira, and A. A. Vicente, J. Food Sci., 2004, 69, C696.

7. F. Icier, H. Yildiz, and T. Baysal, J. Food Eng., 2006, 74, 424.

8. F. Icier, H. Yildiz, and T. Baysal, J. Food Eng., 2008, 85, 410.

9. A. Jakob, J. Bryjak, H. Wojtowicz, V. Illeova, J. Annus, and M. Polakovic, Food Chem., 2010, 123, 369.

10. E. K. Durham. Moderate electric field treatment for saccharification of cellulose materials (Ph.D. Thesis, The Ohio State University, Columbus, OH, 2015).

11 C. P. Samaranayake, and S. K. Sastry, Food Chem., 2016, 199, 265.

12. C. P. Samaranayake, and S. K. Sastry, J Food Eng., 2016, 186, 17.

13. C. P. Samaranayake, and S. K. Sastry, LWT – Food Science and Technology, 2018, 90, 448.

14. G. G. Hammes, S. J. Benkovic, and S. Hammes-Schiffer, Biochemistry, 2011, 50, 10422.

15. A. Kohen, Acc. Chem. Res., 2015, 48, 466.

16. M. Karplus, and J. A. McCammon, Nat Struct Biol., 2002, 9, 646.

17. N. J. English, and C. J. Waldron, Phys. Chem. Chem. Phys., 2015, 17 (19), 12407.

18. N. Todorova, A. Bentvelzen, N. J. English, and I. Yarovsky. J. Chem. Phys., 2016, 144, 085101.

19. N. J. English, and D. A. Mooney. J. Chem. Phys., 2007, 126, 091105.

20. F. Lugli, F. Toschi, F. Biscarini, and F. Zerbetto. J. Chem. Theory Comput., 2010, 6, 3516.

21. P. Marracino, F. Apollonio, M. Liberti, G. d'Inzeo, and A. Amadei. J. Phys. Chem. B, 2013, 117, 2273.

22. A. Amadei, and P. Marracino. RSC Adv., 2015, 5, 96551.

23. P. Marracino, D. Havelka, J. Prusa, M. Liberti, J. Tuszynski, A. T. Ayoub, F. Apollonio, and M. Cifra. Scientific Reports, 2019, 9, 10477.

24. della Valle, P. Marracino, O. Pakhomova, M. Liberti, and F. Apollonio. PLoS ONE, 14 (8), e0221685.

25. L. Astrakas, C. Gousias, and M. Tzaphlidou, J. Appl Phys., 2011, 109, 094702.

26. L. Astrakas, L., C. Gousias, and M. Tzaphlidou, J. Appl Phys., 2012, 111, 074702.

27. A. Singh, S. Munshi, and V. Raghavan, Proteomes, 2013, 1, 25.

28. S. K. Vanga, A. Singh, and V. Raghavan, Innov Food Sci Emerg Technol., 2015, 30, 79.

29. B. H. Vagadia, S. K. Vanga, A. Singh, and V. Raghavan, Innov Food Sci Emerg Technol., 2016, 35, 9.

30. M. J. Abraham, D. van der Spoel, E. Lindahl, B. Hess, and the GROMACS development team, Gromacs User Manual version 5.1.2, 2016, www.gromacs.org.

31. A. Waygood. An Introduction to Electrical Science (Routledge, London, 2018), 2nd Edition, pp 127-143.

32. J. J. Tanner, Acta Cryst., 2016, D72, 1119-1129.

33. M. H. Baig, D. R. Sudhakar, P. Kalaiarasan, N. Subbarao, G. Wadhawa, M. Lohani, M. K. A. Khan, and A. U. Khan, PLoS ONE, 2014, 9 (12): e112456. doi: 10.1371/journal.pone.0112456.

34. A. Cooper, Proc. Natl. Acad. Sci. U.S.A., 1976, 73, 2740.

35. Z. Sun, Q. Liu, G. Qu, Y. Feng, and M. T. Reetz, Chem. Rev., 2019, 119, 1626.

36. D. Zhang, and R. Lazim, Sci. Rep., 2017, 7, 44651, https://doi.org/10.1038/srep44651

37. K. Johansson, M. El-Ahmad, R. Friemann, H. Jornvall, O. Markovic, and H. Eklund, FEBS Lett., 2002, 514, 243.

38. Y. Xie, J. An, G. Yang, G. Wu, Y. Zhang, L. Cui, and Y. Feng, J. Biol. Chem., 2014, 289, 7994.

39. V. B. Chen, W. B. Arendall 3rd, J. J. Headd, D. A. Keedy, R. M. Immormino, G. J. Kapral, L. W. Murray, J. S. Richardson, and D. C. Richardson, Acts Cryst., 2010, D66, 12.

40. S. C. Lovell, I. W. Davis, W. B. Arendall 3rd, P. I. de Bakker, J. M. Word, M. G. Prisant, J. S. Richardson, and D. C. Richardson, Proteins: Struct., Funct., Genet., 2003, 50, 437.

41. S. Bandyopadhyay, S. Chakraborty, and B. Bagchi, J. Am. Chem. Soc., 2005, 127, 16660.

42. M-C. Bellissent-Funel, A. Hassanali, M. Havenith, R. Henchman, P. Pohl, F. Sterpone, D. van der Spoel, Y. Xu, and A. E. Garcia, Chem. Rev., 2016, 116, 7673.

43. S. K. Sinha, and S. Bandyopadhyay, Phys. Chem. Chem. Phys., 2012, 14, 889.

44. R. Zhang, L. Cheng, L. Wang, and Z. Guan, IEEE T PLASMA SCI., 2006, 34, 2630.

45. I. Bekard, and D. E. Dunstan, Soft Matter., 2014, 10, 431.

46. T. Duong, M. Balaban, and C. Perera, J. Food Sci., 2015, 80, E2486.

47. M. Tian, T. Fang, M. Du, and F. Zhang, Protein J., 2016, 35, 154.

48. J. E. Donald, D. W. Kulp, and W. F. DeGrado, Proteins, 2011, 79, 898.

49. L. Guo, J. Park, T. Lee, P. Chowdhury, M. Lim, and F. Ga, J. Phys. Chem. B., 2009, 113, 6158.

50. I. Danielewicz-Ferchmin, and A. R. Frechmin, J. Mol Liq., 2016, 124, 114.

51. E. D. Kirson, V. Dbaly, F. Tovarys, J. Vymazal, J. F. Soustiel, A. Itzhaki, D. Mordechovich, S. Steinberg-Shapira, Z. Gurvich, R. Schneiderman, Y. Wasserman, M. Salzberg, B. Ryffel, D. Goldsher, E. Dekel, and Y. Palti, Proc. Natl. Acad. Sci. U.S.A., 2007, 104, 10152.